



Materials
Horizons

**Chirality and Dislocation Effects in Single Nanostructures
Probed by Whispering Gallery Modes**

Journal:	<i>Materials Horizons</i>
Manuscript ID	MH-COM-05-2023-000693.R1
Article Type:	Communication
Date Submitted by the Author:	28-Jun-2023
Complete List of Authors:	Sutter, Peter; University of Nebraska-Lincoln, Electrical and Computer Engineering Khosravi-Khorashad, Larousse; University of Nebraska-Lincoln, Electrical and Computer Engineering Ciobanu, Cristian; Colorado School of Mines, Division of Engineering Sutter, Eli; University of Nebraska-Lincoln, Department of Mechanical and Materials Engineering

SCHOLARONE™
Manuscripts

Chirality and Dislocation Effects in Single Nanostructures Probed by Whispering Gallery Modes

New Concepts

We demonstrate chiral optical effects and dislocation-induced electronic modifications that can transform semiconductor nanostructures into multifunctional components for optoelectronics and photonic circuitry. The work overcomes two key challenges: The controlled synthesis of inorganic nanostructures that are chiral and carry a single electronically active defect; and the detection of chirality and dislocation effects in individual nanostructures rather than ensembles. To address the first challenge, we developed a growth process, which yields thick, tapered van der Waals semiconductor nanowires that consistently incorporate an axial screw dislocation. Using a suitable thermal protocol during growth, the resulting chiral growth spiral making up a large part of each wire is joined to a non-dislocated (achiral) section, hence enabling the direct comparison of the properties of chiral and achiral segments within the same nanostructure. And whereas conventional chiroptic measurements, such as circular dichroism, can be applied only to larger chiral ensembles, we introduce optical whispering gallery modes as a new probe of chirality and dislocation effects in single nanostructures. The results open up a field of research aimed at harnessing nanostructures with inherent chirality and defect-derived functionality for applications such as light emission and detection, sensing, and information processing.

Chirality and Dislocation Effects in Single Nanostructures Probed by Whispering Gallery Modes

Peter Sutter,^{1,*} Larousse Khosravi-Khorashad,¹ Cristian V. Ciobanu,² and Eli Sutter^{3,4,*}

¹Department of Electrical and Computer Engineering, University of Nebraska-Lincoln, Lincoln, NE 68588, United States

²Department of Mechanical Engineering, Colorado School of Mines, Golden, CO 80401, United States

³Department of Mechanical and Materials Engineering, University of Nebraska-Lincoln, Lincoln, NE 68588, United States

⁴Nebraska Center for Materials and Nanoscience, University of Nebraska-Lincoln, Lincoln, NE 68588, United States

*To whom correspondence should be addressed, e-mail: psutter@unl.edu, esutter@unl.edu

Abstract

Nanostructures such as nanoribbons and –wires are of interest as components for building integrated photonic systems, in particular if their basic functionality as dielectric waveguides can be extended by chiroptical phenomena or modifications of their optoelectronic properties by extended defects, such as dislocations. However, conventional optical measurements typically require monodisperse (and chiral) ensembles, and identifying emerging chiral optical activity or dislocation effects in single nanostructures has remained an unmet challenge. Here we show that whispering gallery modes can probe chirality and dislocation effects in single nanowires. Wires of the van der Waals semiconductor germanium (II) sulfide (GeS), obtained by vapor-liquid-solid growth, invariably form as growth spirals around a single screw dislocation that gives rise to a chiral structure and can modify the electronic properties. Cathodoluminescence spectroscopy on single tapered GeS nanowires containing joined dislocated and defect-free segments, augmented by numerical simulations and *ab-initio* calculations, identifies chiral whispering gallery modes as well as a pronounced modulation of the electronic structure attributed to the screw dislocation. Our results establish chiral light-matter interactions and dislocation-induced electronic modifications in single nanostructures, paving the way for their application in multifunctional photonic architectures.

1. Introduction

Chiral optics, optoelectronics, and photonics can provide functionality beyond that of conventional optics with broad applications including sensing,^{1, 2} communication,^{3, 4} information processing,^{5, 6} *etc.* Although individual molecules and nanoscale objects can adopt chiral structures or morphologies that affect their interaction with light, most implementations to date have focused on ensembles to obtain measurable effects. This is true for molecular ensembles such as cholesteric liquid crystals,⁷ as well as for metamaterials and metasurfaces comprising arrays of plasmonic⁸ or dielectric nanostructures.⁹ The availability of monolithic nanostructures with chiral light-matter interactions could pave the way for integrated photonic systems, for example chiral waveguides containing quantum emitters¹⁰ that generate circularly polarized single photons with definite handedness for quantum communication or cryptography. Prior theoretical results suggested that screw dislocations can bestow chirality onto single dielectric nanostructures¹¹ and give rise to giant optical activity.¹² By inducing tunable Eshelby twist,¹³ screw dislocations in van der Waals nanowires also provide an avenue toward realizing precision small-angle interlayer twist and associated twist moiré patterns.^{14, 15} Such moiré structures, which incorporate a distinct handedness, offer another avenue toward chiral light-matter interactions.^{16, 17} In addition to inducing chirality, dislocations have been predicted to give rise to distinct functional properties in their host crystal, including highly coherent spin textures,¹⁸ Majorana bound states,¹⁹ chiral anomalies in Dirac semimetals,^{20, 21} and low-dimensional gapless modes in topological insulators.²² Recent theoretical work established a framework for treating dislocations as quantized quasiparticles (*'dislons'*) analogous to phonons,^{23, 24} leading to predictions of other dislocation-induced properties including an oscillatory electron energy near a dislocation core,²⁵ effects on phonons,²⁶ and dislocation-induced superconductivity.²⁷ However,

the detection of such emerging phenomena and their unambiguous association with dislocations has remained a major challenge.

Here, we show that whispering gallery photonic modes are a sensitive probe of chirality and dislocation effects by combining experiments and simulations for nanowires of the van der Waals semiconductor germanium (II) sulfide (GeS), synthesized by a vapor-liquid-solid (VLS) process.²⁸ A large majority of the as-grown nanowires host an axial screw dislocation. The dislocation with predominant Burgers vector of magnitude 1.04 nm (*i.e.*, the *c*-lattice constant of GeS) causes multiple modifications of structure and properties. Firstly, it gives rise to a helical structure of the nanowires, which are, in fact, growth spirals around the screw dislocation.²⁹⁻³¹ Secondly, the dislocation and the associated Eshelby twist (induced by a torque on the ends of a cylindrical solid due to the stress field of an axial screw dislocation)^{13, 14, 32} cause a progressive rotation of the in-plane (*a*, *b*) crystal axes at a rate that is tunable *via* the nanowire diameter, which for a layered material translates into a small-angle interlayer twist and associated twist moiré pattern at the van der Waals interface between adjacent turns of the helical wires (Figure 1a).¹⁴ And thirdly, the screw dislocation can modify the electronic structure, charge transport, thermal, spin, and topological properties. The controlled ejection of the screw dislocation during growth¹⁵ produces a homojunction connecting the chiral (twisted) base of each wire to an achiral (layered) segment near the tip (Figure 1b). The presence of dislocated and defect-free structures in the same nanowire provides a basis for identifying chiroptic effects due to the helical structure, as well as probing electronic effects due to the twist moiré or the axial screw dislocation.

2. Results and Discussion

Circular dichroism in single chiral twisted GeS nanowires

The conventional measure of far-field chiroptical effects involves the circular dichroism (CD), *i.e.*, the difference in the interaction with left- and right-circularly polarized light.^{33, 34} In

chiral GeS nanowires, two different effects contribute to the CD:³⁵ (i) the structure of the wires in the form of helical growth spirals around an axial screw dislocation; and (ii) the continuous rotation of the crystal axes along the wires due to Eshelby twist. We carried out numerical simulations (see Methods) of the CD in absorption, scattering, and extinction for a segment of a helical GeS nanowire with helix pitch ranging from 10 nm to 3.5 nm (Figure S1). The CD, expressed here as an absorption, scattering, or extinction cross section, generally shows a pronounced peak at 1.8 eV, followed by smaller peaks at higher energy, and a linearly decreasing cross section as a function of the simulated pitch of the helix. Extrapolation of this linear dependence shows a finite residual CD at the actual ~ 1 nm pitch of the chiral twisted GeS nanowires (*i.e.*, 1.04 nm Burgers vector of the axial screw dislocation)^{14, 15, 36} realized by VLS growth. However, accessing this chiroptical response experimentally *via* far-field CD measurements poses considerable challenges, associated with measuring the interaction of light with single chiral nanostructures or the need for special growth protocols to transform racemic mixtures of left- and right-handed helices into chiral ensembles. To overcome these challenges, we explored the possibility of using photonic modes – in particular whispering gallery modes, *i.e.*, traveling waves that propagate along the boundary between a convex-shaped object with high refractive index and a lower-index medium – to detect chirality effects in single nanowires.

Chiral twisted GeS nanowires as resonators carrying whispering gallery modes

Whispering gallery modes (WGMs) were first identified by Lord Rayleigh in the form of acoustic (pressure) waves traveling along the circular gallery of London's St. Paul's cathedral.³⁷ Their optical analogue can be implemented with different cavity designs such as, for example, microsphere, microdisk or microtoroid resonators with diameters in the range from a few μm to

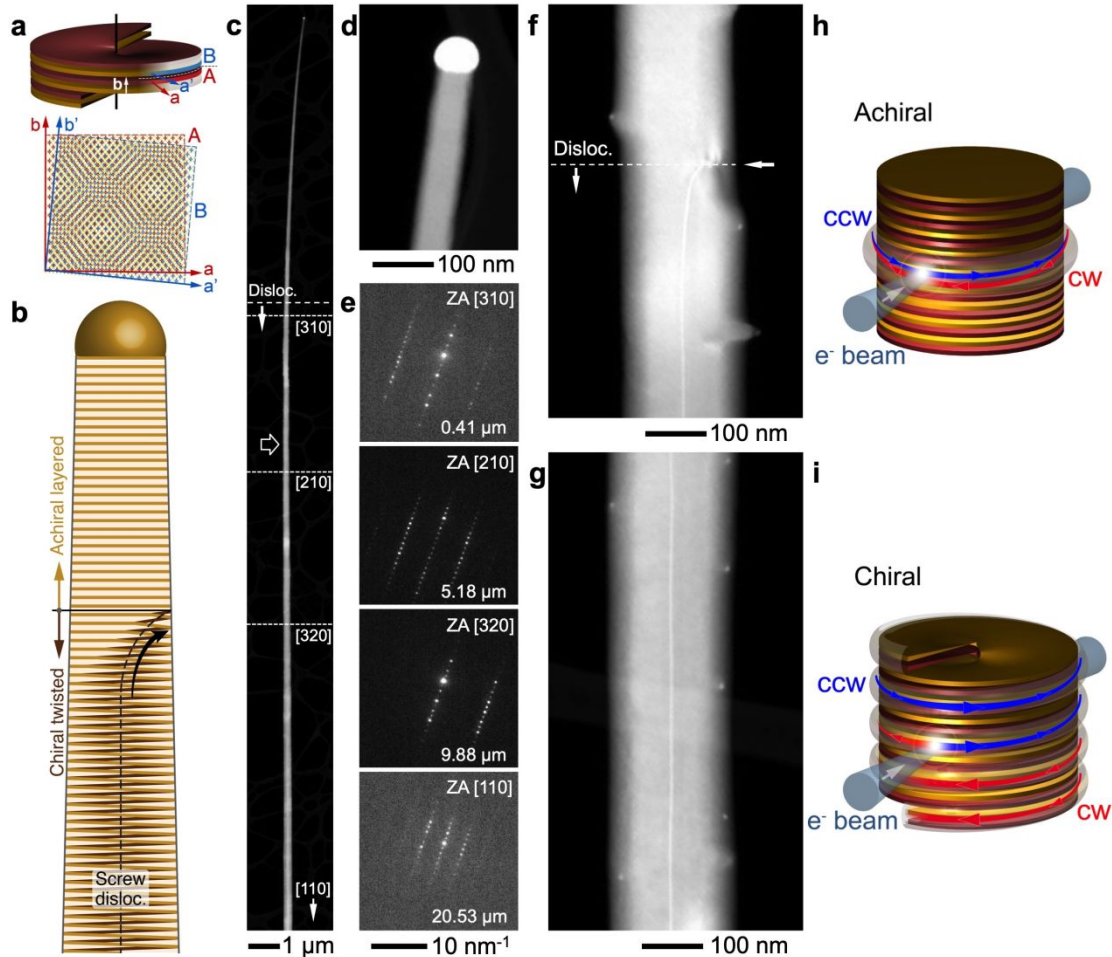


Figure 1. Tapered GeS chiral twisted van der Waals nanowires. **a.** Schematic of the helical structure of the dislocated GeS nanowires. Eshelby twist introduces a controlled interlayer twist at the van der Waals interface between adjacent turns of the helix (A, B), thus producing a twist moiré projected onto the helicoid interface along the nanowires (bottom). **b.** Schematic of a van der Waals nanowire incorporating a junction connecting an achiral segment near the tip to a chiral twisted segment at the base. **c.** HAADF-STEM image of a tapered nanowire obtained by Au-catalyzed VLS growth from mixed GeS and SnS precursors at 240°C. The tip section of the wire is achiral; the segment below the dashed line ('Disloc.') carries an axial screw dislocation, *i.e.*, is chiral. **d.** STEM image showing the VLS catalyst at the nanowire tip. **e.** Position-dependent nanobeam electron diffraction showing a progression between different local zone axes (ZA) in the dislocated (chiral) segment, as specified in c. Indicated distances reflect the separation of the diffraction pattern from the point of dislocation ejection. **f.** STEM image obtained near the point at which the axial screw dislocation emerges from the nanowire. **g.** STEM image obtained in the dislocated segment (horizontal arrow in c.). **h.** Excitation of clockwise (cw) and counterclockwise (ccw) whispering gallery modes in an achiral van der Waals nanowire by the focused electron beam in STEM. **i.** Chiral whispering gallery modes with separated cw and ccw propagating waves in a twisted van der Waals nanowire.

few tens of μm , to which light is confined by total internal reflection and where light is coupled in/out using a proximal fiber waveguide.³⁸ WGMs have also been observed in cylindrical solids,

such as nanowires and –rods of semiconductors such as Si,³⁹ ZnO,⁴⁰ and GaN.⁴¹ Here, tapered geometries provide access to a continuously varying cavity size/diameter, and the resulting dispersive WGMs are usually probed by local excitation using a focused electron beam and detection of light emitted from the resonator by cathodoluminescence (CL, see for example Ref. 40).

For nanowires of layered semiconductors such as GeS (relative permittivity $\epsilon_r \approx 12$ for visible/near-infrared light),⁴² WGMs of order $N \geq 2$ are supported at diameters greater than ~ 100 nm. Tapered nanowires facilitate the identification of WGMs *via* their characteristic dispersion with the resonator diameter. VLS growth from a pure GeS precursor over Au catalysts yields nanowires with diameters between ~ 30 -120 nm in a narrow substrate temperature window ($300 \pm 5^\circ$).¹⁴ To realize thick, tapered GeS nanowires, a VLS protocol was developed where SnS vapor was added to the main GeS growth precursor (see Methods for details). The added SnS vapor achieved two modifications: (i) An expansion of the temperature window for nanowire growth down to $\sim 240^\circ\text{C}$, making the growth process more robust; and (ii) the synthesis of thick (up to ~ 400 nm), tapered chiral nanowires. Nearly all ($>95\%$) of the nanowires obtained with this growth protocol contained an axial screw dislocation. A sharp drop in the sample temperature near the termination of the growth caused the ejection of the dislocation followed by growth of a final defect-free part of the nanowire with typical length of several μm , *i.e.*, introduced a twist homojunction between the dislocated base and a non-dislocated segment near the tip.¹⁵

Chemical analysis shows that the resulting nanowires remain close to pure GeS, *i.e.*, the added SnS acts as a growth modifier that is incorporated only in trace amounts (< 1 at. %, see Figure S2). A typical nanowire is shown in Figure 1c-g. Figure 1c shows a high-angle annular dark-field scanning transmission electron microscopy (HAADF-STEM) image of a long, tapered

GeS nanowire consisting of an achiral segment of ~ 8.8 μm length near the tip, followed by a substantially longer chiral segment hosting an axial screw dislocation. Figure 1d, a STEM image of the nanowire tip terminated by the Au-rich catalyst particle, confirms VLS growth from mixed GeS/SnS vapors at 240°C . Nanobeam electron diffraction patterns (Figure 1e) are consistent with Eshelby twist¹³ in the dislocated parts of the nanowires, which causes a continuous rotation of the nanowire between different zone axes (here from $[310]$ to $[110]$, see Figure 1c), confirming the chiral structure. HAADF-STEM images illustrate the morphology at the junction where the axial screw dislocation is expelled from the nanowire (Figure 1f) and within the dislocated segment toward the base of the wire (Figure 1g). In both cases, the axial screw dislocation is clearly visible as a narrow line with bright scattering contrast.⁴³

The thick GeS nanowires with diameters of $\sim 100 - 400$ nm realized here act as resonators carrying whispering gallery modes (WGMs), similar to nanowires and -rods of other semiconductors such as Si,³⁹ ZnO,⁴⁰ GaN,⁴¹ *etc.* In contrast to these conventional 3D-crystalline semiconductors, our 2D (van der Waals) nanowires with twist homojunctions present two distinct structures: Layered GeS near the tip, connected to a chiral twisted segment toward the base. Excitation by the focused electron beam in STEM induces localized fields that can selectively excite WGMs in small parts along each segment. In the defect-free achiral segment, the beam is expected to induce counterpropagating WGMs, analogous to ordinary semiconductor nanowires (Figure 1h). In the dislocated chiral segment, on the other hand, the WGMs experience the helical and twisted layer structure (Figure 1i), which may cause a spatial separation of clockwise (cw) and counterclockwise (ccw) propagating modes and other chirality-induced effects. To detect these effects, we collected emitted light from the WGMs using cathodoluminescence (CL) spectroscopy.⁴⁰

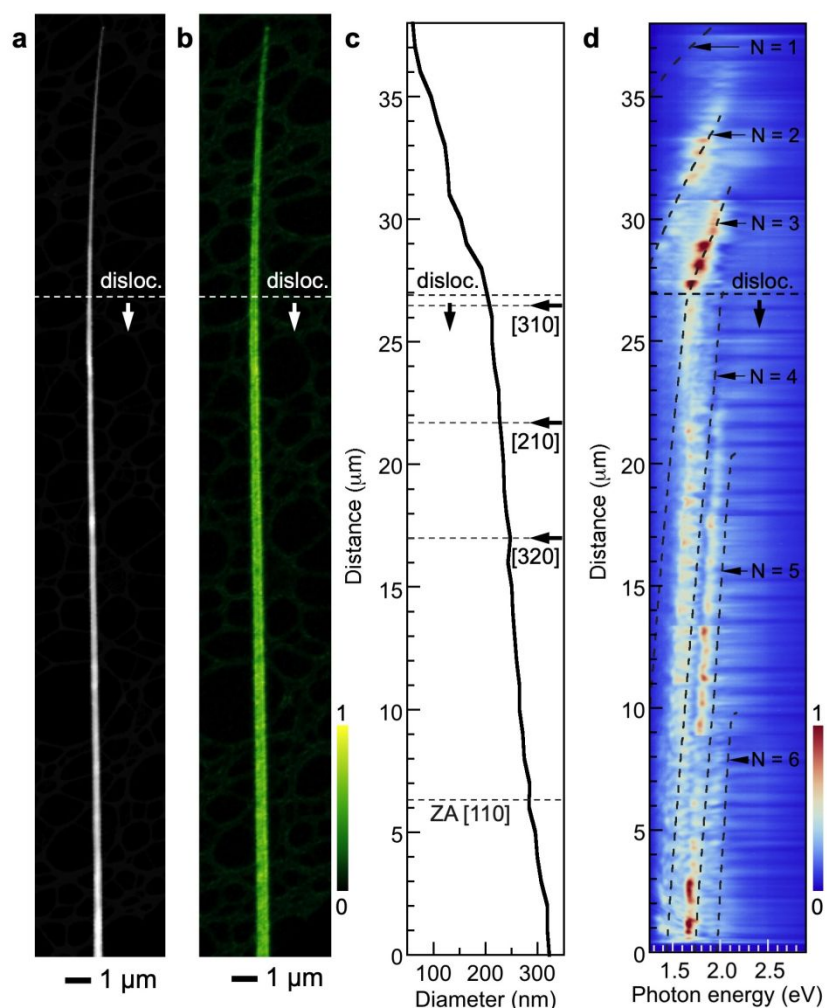


Figure 2. Whispering gallery modes (WGMs) in tapered GeS van der Waals nanowires. **a.** HAADF-STEM image of a tapered nanowire obtained by Au-catalyzed VLS growth from mixed GeS and SnS precursors at 240°C. **b.** Panchromatic STEM-CL map of the nanowire shown in **a.** Right: False color intensity scale (arb. units). **c.** Position-dependent nanowire diameter determined from the STEM image in **a.** In the dislocated segment, selected low-index zone axes (ZA) of the electron beam (determined by nanobeam diffraction) are indicated. **d.** Hyperspectral STEM-CL linescan along the central axis of the nanowire in **a.** Right: False color intensity scale (arb. units). Overlays represent plane-wave simulations of the light emission from $N = 1 - 6$ WGMs using the optical constants of GeS, assuming a mode diameter equal to the position-dependent diameter of the tapered nanowire (as shown in **c.**).

Figure 2 summarizes the analysis of a long GeS nanowire using combined STEM imaging and STEM-CL spectroscopy. The nanowire morphology imaged by HAADF-STEM is illustrated in Figure 2a. The tapered wire expands from a diameter of ~ 80 nm near the tip to over 300 nm near its base. A junction ~ 9 μm from the tip joins the non-dislocated near-tip segment from the dislocated base of the nanowire. The panchromatic CL map of Figure 2b demonstrates intense,

uniform light emission from the wire excited by the focused electron beam in STEM. The diameter profile and the changing crystal orientation of the twisted wire (reflected by a progressive rotation of the local zone axis, ZA) are given in Figure 2c. Figure 2d shows a hyperspectral STEM-CL linescan along the entire GeS nanowire, in which the color scale represents the local intensity of emitted light as a function of photon energy. For most positions, the measurement shows several intensity maxima whose peak photon energy systematically changes with the nanowire diameter. Dashed lines indicate the energy of whispering gallery modes calculated with a plane-wave model (in which successive orders N of WGMs correspond to integer numbers of mode wavelengths λ matching the circumference of the cylindrical cavity)⁴⁰ using the optical constants of GeS,⁴² with resonator diameter equal to the wire diameter measured by STEM (Figure 2c). While the mode dispersion is generally well reproduced, the calculated modes do not match everywhere with the peak photon energies detected by CL. In the non-dislocated (achiral) segment of the nanowire, the calculated WGM energies correspond closely with experiment. In the dislocated (chiral) segment, on the other hand, the model fails to describe the experimentally observed emission spectra. In particular, the peak photon energy of the emitted light appears to be systematically blue-shifted compared to the calculated WGM energy.

Identification of chiral whispering gallery modes

Additional numerical simulations were performed to corroborate the departure of WGMs in chiral parts of the GeS wires from the expected dispersion, and to identify the mode structure and the selection rules for excitation by the electron beam (Figure 3). The simulations used a strip waveguide tangential to a nanowire (Figure 3a) to excite WGMs, whose energies can be identified *via* minima in the transmission of the waveguide. Simulated transmission

characteristics for an achiral GeS nanowire with dimensions equal to those shown in Figure 2c are given in Figure 3c and Figure 3d for excitation by E_z and E_x polarized plane waves, respectively. The spectra contain a series of transmission minima that indicate the excitation of match the experimental WGM energies in the achiral part of the wire, while the E_z excitation

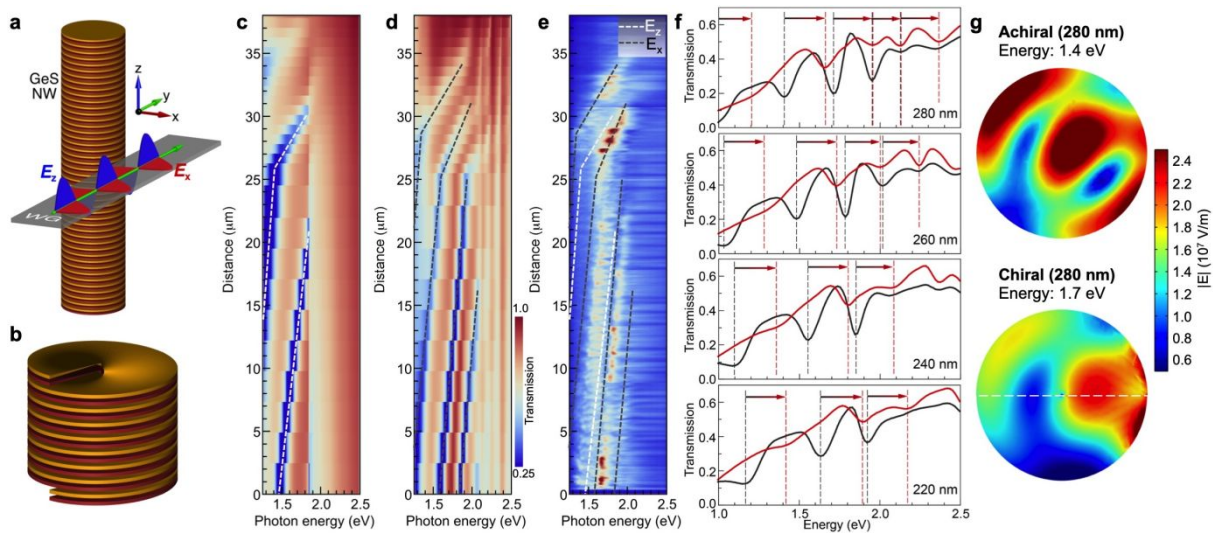


Figure 3. Numerical simulations of WGMs in GeS nanowires. **a.** Schematic of the configuration used for Comsol simulations, involving excitation of WGMs in a GeS nanowire (NW) by a tangential strip waveguide (WG) carrying an incoming wave with electric field along z (E_z , TM polarization) or along x (E_x , TE polarization), respectively. **b.** Geometry of the dislocated GeS nanowires used for 3D Comsol modeling of WGMs in chiral wires. **c.** Simulated transmission of the strip waveguide for E_z excitation of an achiral GeS wire. **d.** Simulated transmission of the strip waveguide for E_x excitation of an achiral GeS wire. Transmission minima in panels c. and d. coincide with energies at which a WGM is excited in the adjacent GeS nanowire. The geometry of the simulated tapered nanowire is identical to that of the wire shown in Figure 2. **e.** Comparison of the simulations for E_z and E_x excitation with a STEM-CL linescan (see Figure 2d). **f.** Comparison of simulated transmission curves of a strip waveguide adjacent to an achiral (black) and chiral (red) GeS nanowire for wire diameters between 220 nm and 280 nm. Arrows mark the blue shift of the transmission minima (*i.e.*, WGM energies) in the chiral wire. **g.** Absolute value of the electric field in a nanowire (diameter: 280 nm) plotted at corresponding WGM energies as shown in panel f., for an achiral wire (top) and a chiral wire (bottom). The exciting strip waveguide is located on the right edge of the wire.

yields a poor correspondence overall. This suggests that the electron beam in our experiments excites E_x polarized WGMs, consistent with selection rules under which the excitation is most efficient for modes with electric field parallel to the electron trajectory (Figures S3, S4).⁴⁴ And secondly, while the simulations for E_x polarization reproduce the experiment in the achiral

segment near the nanowire tip, the measured WGMs in the chiral part of the wire are consistently blue-shifted compared to the simulations. Figure S5 shows the same pronounced blue shift of the experimentally observed WGMs relative to the energies calculated within a plane wave model.

To corroborate this observed behavior of the photonic modes in chiral nanowires, we carried out numerical simulations in a three-dimensional (3D) geometry explicitly taking into account the helical structure (Figure 3b). Due to the computational cost, the simulations were limited to four different wire diameters for which we compared the transmission characteristics of a strip waveguide adjacent to an achiral and chiral nanowire resonator (Figure 3f). The calculations for wire diameters ranging from 220 nm to 280 nm show the same behavior, namely overall similar transmission with pronounced minima (corresponding to WGM resonances) for both achiral (Figure 3f, black curves) and chiral resonators (Figure 3f, red curves); and a consistent blue shift of the WGM energies in the chiral GeS nanowires compared to achiral wires (arrows). The shift in WGM energy in chiral nanowires is further substantiated by 3D simulations of the electric field distributions in achiral and chiral wires (Figure 3g). Plots of the fields in the (x, y) plane inside a 280 nm wire at energies of 1.4 eV and 1.7 eV, corresponding to WGMs in achiral and chiral wires, respectively, as determined from Figure 3f, show a close correspondence in the mode pattern within the wires. This confirms that the mode in the chiral wire is indeed blue-shifted (here by ~ 0.3 eV) from the lower-energy mode in the achiral geometry. From the combined experimental and simulation results, we conclude that a pronounced blue shift of the mode energies at all diameters of the resonator is a telltale signature of chiral WGMs.

The physical origins of this effect merit additional discussion. Chiral signatures detected by circular dichroism (CD) spectroscopy (measuring the difference in the absorption of right- and left-circularly polarized light, see Figure S1) can be understood in terms of a coupled exciton

model. Transitions to excitonic states of a chiral array of chromophores (or other centers supporting an electronic transition) are excited to differing extents by right- and left-circularly polarized light, thereby producing bisignate curves (so-called exciton couplets) in their CD spectra.⁴⁵ Prior theoretical results showed that modifications of the permittivity tensor by screw dislocations and Eshelby twist in objects such as nanowires/rods, quantum dots, and nanodisks can also give rise to CD.³⁵ While the presence of a screw dislocation results in CD only if the underlying crystal is anisotropic, Eshelby twist, (*i.e.*, a progressive lattice rotation around the dislocation)¹³ invariably induces chirality. Similar effects are also expected in other geometries, *e.g.*, twisted nanoribbons.⁴⁴ Our results suggest that in chiral structures supporting WGMs, such as nanowires or -rods with screw dislocations, the altered permittivity tensor manifests itself in a systematic shift of the mode energies, in our case towards higher energy. To support this conclusion, we note that the blue shift of the WGMs is indeed a perturbative effect, *i.e.*, the same modes exist in achiral and chiral wires (see also Figure 3g) but they are shifted to higher energy in the chiral parts. This can be seen by comparing numerical simulations of WGMs in helical wires with the same diameter but different helix pitch, as shown in Figure S10 where the shifts of the WGM energies scale with the pitch (*i.e.*, the magnitude of the Burgers vector, **b**) of the helical wires. Within a plane-wave model, the observed mode shift to higher energies is consistent with an increase in the effective refractive index in the chiral part of the nanowires, suggesting distinct (effective) optical constants modified by the chiral structure and Eshelby twist.

Whispering gallery modes as a probe of dislocation effects

Apart from the shift in the WGMs carried by chiral resonators, chiral van der Waals nanowires have two other unusual properties compared to conventional (3D-crystalline)

semiconductor nanowires: (i) each nanowire carries a single axial screw dislocation over most of its length; and (ii) the dislocation causes Eshelby twist, which for a layered nanowire gives rise to an interlayer twist moiré projected onto a helicoid van der Waals interface (see Figure 1a). Such nanowires are therefore expected to host a modulated electronic structure due to a changing moiré registry along the wire^{14, 15} as well as direct dislocation effects (Figures S6, S7).²³⁻²⁵ In thin nanowires with large Eshelby twist, several different moiré registries are traversed even along short (few μm) sections, so that the two competing effects are difficult to disentangle. As illustrated in Figure S8, this issue can be overcome in thicker wires. In GeS nanowires with ~ 300 nm diameter, a single moiré registry is maintained over several μm length along the wires. Hence, modulations in the electronic structure of such thick nanowires, detected *via* WGMs and identified by direct comparison between dislocated and defect-free nanowires of the same diameter, can be unambiguously assigned to effects of the axial screw dislocation.

Analogous to WGM microdisk lasers, where stimulated emission occurs at resonance between a cavity mode and an optical transition of the gain medium (*e.g.*, a III-V⁴⁶ or III nitride⁴⁷ quantum well structure), light emission in CL of nanorods or nanowires carrying WGMs requires the coupling between the photonic modes and the radiative recombination between electronic states in the semiconductor. Multiple WGMs can be accessed in materials that support a continuum of radiative transitions, such as the defect band that gives rise to green luminescence within the bandgap of hexagonal ZnO nanorod cavities.^{40, 48} A similar situation is realized in GeS. CL spectra from bulk GeS flakes show a dominant band-edge luminescence peak (at ~ 1.62 eV) and a broad shoulder due to light emission across a continuum of lower energies within the GeS bandgap (Figure 4a). Luminescence from this continuum of radiative transitions enables the analysis of different WGMs along the GeS nanowires by CL (see Figure 2, Figure 3).

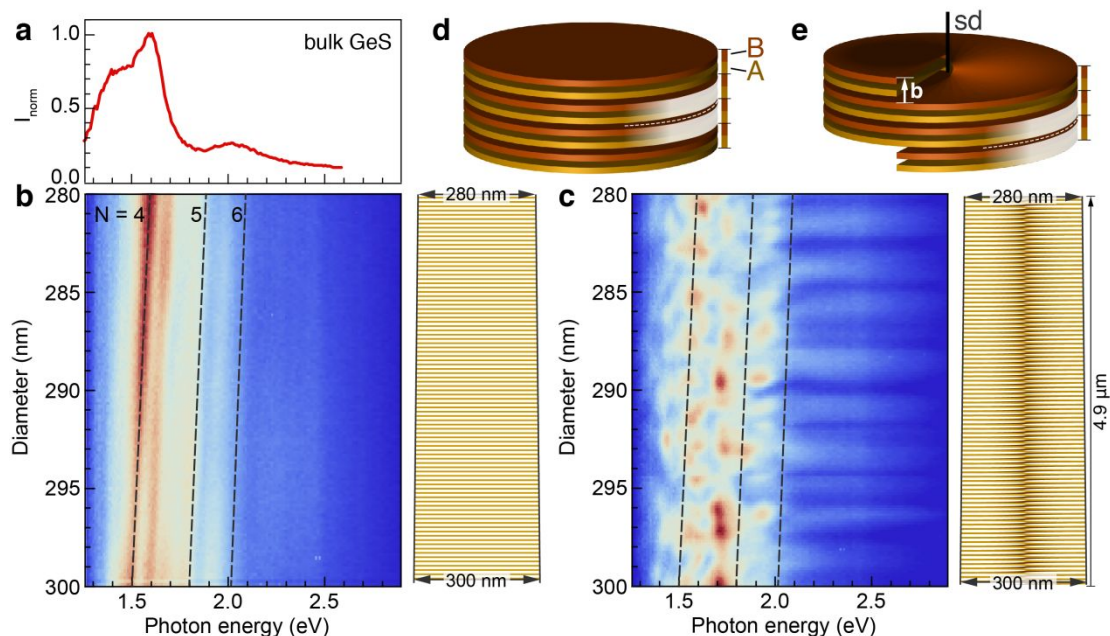


Figure 4. CL linescans along defect-free and dislocated nanowires of equal thickness. **a.** Reference spectrum of a bulk GeS flake, showing a band-edge peak at ~ 1.60 eV as well as a broad shoulder to lower energies. **b.** Hyperspectral CL linescan along a tapered defect-free GeS nanowire (schematic in **d.**) covering diameters between 280 – 300 nm. Dashed lines mark the dispersion of WGMs with $N = 4$ to 6, calculated using a plane-wave model. Right: Illustration of the tapered layered nanowire segment. **c.** Hyperspectral CL linescan along a segment of a dislocated GeS nanowire (schematic in **e.**) covering the same range of diameters. Dashed lines are identical to those shown in **b.** Right: Illustration of the tapered dislocated nanowire segment. **d.** Layer structure of the defect-free GeS nanowire with equilibrium AB layer stacking. **e.** Dislocated GeS nanowire with Burgers vector \mathbf{b} of the axial screw dislocation (sd).

Hyperspectral CL linescans along defect-free tapered GeS nanowires show several bands corresponding to light emission from WGMs (Figure 4b). The intensity of the emitted light increases as the WGMs (*e.g.*, the $N = 4$ mode in Figure 4b) approach the GeS bandgap energy, *i.e.*, come to resonance with the fundamental bandgap of the semiconductor host. This increase in intensity toward resonance is accompanied by a decrease in the WGM quality factor, here from $Q \sim 35$ at 1.5 eV photon energy to $Q \sim 10$ at the bandgap energy (Figure S9), consistent with an increased absorption and damping of the WGM.

In the dislocated nanowire of the same composition and geometry, obtained in the same synthesis run, the continuous emission bands seen in Figure 4b break up into distinct peaks alternating with areas of low emission intensity (Figure 4c). The emission maxima cover the

entire energy range traversed by WGMs in this segment of the wire, *i.e.*, $\sim 1.4 - 2.0$ eV. The most intense maxima are slightly blue-shifted from the band edge of bulk GeS (~ 1.62 eV, Figure 4b) to ~ 1.7 eV (Figure 4c). This shift in *emission energy* relative to the bulk bandgap may be explained by a moiré effect, *i.e.*, the moiré registry present in the segment shown in Figure 4c appears to be one with an increased bandgap (see Figure S6). However, given the constant moiré registry along the ~ 4.9 μm section covered by the CL linescan (Figure S8), we can rule out moiré effects as the cause for the *modulated light emission*. Hence, we are compelled to consider alternative explanations in terms of direct dislocation effects on the electronic structure. A possible origin may be trapped charges along the dislocation core, as found for screw dislocations in oxides,^{49, 50} whose random distribution may explain the rapidly changing energy landscape probed by WGMs along the dislocated GeS wires. Other possible explanations involve a modulation of the electron energy by the dislocation. Recent calculations have predicted an oscillatory electron energy in the vicinity of both edge- and screw dislocations.⁵¹ The predicted anisotropy of the electron self-energy near the dislocation as well as large variations within tens of nanometers around the dislocation core are consistent with the fluctuations observed in our CL linescan (Figure 4c), in particular if small deviations from a circular resonator cross-section cause ray trajectories that traverse the interior of the nanowire at varying distance from the dislocation.⁵² While additional work is needed to unambiguously identify the origin of the observed modulation, our measurements demonstrate that whispering gallery modes provide a powerful tool for probing the energy landscape along dislocated nanostructures, enabling the detection and investigation of electronic effects of single dislocations.

3. Conclusions

Experiments using cathodoluminescence combined with numerical simulations showed effects of chirality and of screw dislocations on whispering gallery modes carried by van der Waals nanowires. A comparison between chiral and achiral segments along single nanowires identifies a blue shift of the modes as the primary effect of a chiral twisted structure. This result represents a long-sought experimental confirmation of theoretically predicted screw dislocation-induced chirality,^{11, 12} and it highlights the power of whispering gallery modes – here excited by a nanometer-focused electron beam and analyzed *via* cathodoluminescence spectroscopy of the emitted light – for probing chirality effects in single dielectric nanostructures. While our measurements focused on nanowires with a helical structured and Eshelby twist resulting from an axial screw dislocation, similar measurements could be applied to investigate chiral light-matter interactions arising through other mechanisms, *e.g.*, decoration with chiral molecules, chiral assemblies of nanoparticles or other nanostructures on the surface,⁵³ *etc.*

Furthermore, we showed that besides measuring chirality effects in single nanostructures, whispering gallery modes can also probe local variations of the electronic structure and optoelectronic properties at the nanoscale. Such measurements, which also use excitation of the photonic modes by a focused electron beam along with far-field light collection, are based on the dependence of the emitted light intensity on the energy overlap between the whispering gallery modes and electronic transitions in the dielectric host medium. By comparing light emission from dislocated and defect-free nanowires with the same composition and diameter and excluding possible other effects, *e.g.*, due to a varying moiré registry along the layered nanowires,¹⁴ our measurements detect fluctuations in the emission that we associate with a modulation of the electronic structure near a single screw dislocation. While the present study

focused on nanowires of layered crystals, the same approach may be applied to nanostructures of 3D-crystalline semiconductors to investigate dislocation effects in a variety of host materials. Future work could harness additional capabilities of cathodoluminescence in both STEM and scanning electron microscopy, *e.g.*, ultrafast/time resolved CL or measurements using structured electron beams,⁵⁴ to uncover the functional properties of dislocations and other defects.

Materials and Methods

Synthesis of tapered, large-diameter GeS nanowire resonators: Thick, tapered GeS nanowires were synthesized by vapor-liquid-solid (VLS) growth by simultaneous vapor transport from two powder precursors, GeS (99.99%, Sigma Aldrich) and SnS (99.99%, Sigma Aldrich), in a pumped quartz tube reactor with two temperature-controlled zones. The substrates were Si(100) wafers covered by sputtering at room temperature with thin (2-4 nm) Au films, which dewetted at the growth temperature and served as the VLS catalyst. The first (upstream) zone of the reactor containing SnS powder (50 mg) in a quartz boat was heated to 650°C while a second quartz boat with GeS powder (20 mg), located outside the first zone, was heated to 450°C. These conditions result in vapor pressures of ~250 mTorr for GeS (at 450°C) and ~60 mTorr for SnS (at 650°C).⁵⁵ The sample was held in the second (downstream) temperature-controlled zone heated to 240°C. During growth, the quartz reactor was pumped by a mechanical pump and a carrier gas (Ar, 99.9999) flow was maintained at 60 standard cubic centimeters per minute (sccm) at a pressure of 20 mTorr. The reactor temperatures were ramped so that the temperature setpoints were reached simultaneously and held for a growth time of 5 minutes, followed by natural cooling to room temperature. The growth resulted in the formation of nanowires with lengths of several tens of micrometers. A large majority of the wires contained axial screw dislocations along most of their length. The non-dislocated segments near the nanowire tips or occasional wires that were defect-free over their entire length served as reference samples to identify chirality and dislocation effects.

Electron microscopy, nanobeam electron diffraction, and energy dispersive X-ray spectroscopy (EDS): Transmission electron microscopy (TEM), scanning transmission electron microscopy (STEM), and nanobeam electron diffraction were performed in a FEI Talos F200X microscope at an electron energy of 200 keV. Samples consisted of nanowires dry-transferred onto lacey

carbon grids. STEM-EDS maps and EDS spectra were collected using a JEOL NeoARM (S)TEM operating at 80 kV.

Cathodoluminescence spectroscopy in STEM (STEM-CL): Cathodoluminescence spectroscopy was performed in STEM mode using a Gatan Vulcan CL holder at room temperature, 200 keV electron energy and 380 pA incident electron beam current. Panchromatic CL maps were obtained by measuring broadband (400 – 1000 nm wavelength) light emission across 512×512 pixel images with integration times of 1.28 ms per pixel. Hyperspectral linescans were acquired by displacing the focused electron beam in predefined equal steps along single tapered nanowires and acquiring full CL spectra (integration time: 10 s per spectrum) at each beam position.

Numerical simulations: The finite element method using COMSOL Multiphysics software was employed to calculate the optical activity of chiral and achiral nanowires. Calculations of electromagnetic response for chiral nanowires were carried out in 3D *via* full field in the frequency domain. For achiral nanowires with axial symmetry, a 2D geometry was used to realize faster, less computationally intensive calculations. The published bulk permittivity of GeS was used for the nanowire simulations.^{42, 56} To compute whispering gallery mode (WGM) energies for different nanowire diameters, nanowires were aligned with their symmetry axis along the z-axis. Port excitation of a strip waveguide adjacent to the nanowires was used to detect the WGMs, as shown in Figure 3. Two different excitation polarizations were applied, with electric field along the x- and z-axes (denoted in the text as E_x (TE) and E_z (TM) excitation). Scattering boundary conditions were used to prevent backscattered waves into the simulation domain. The transmission (T) and reflection (R) of the waveguide were then calculated *via* the electromagnetic power flow. The absorption (A) of the nanowire was obtained as $A = 1 - T - R$.

To calculate the circular dichroism (CD) of the chiral nanowire, the wire was aligned along z-axis in air as the ambient medium. Both right and left circularly polarized lights (RCP/LCP), propagating along the z-axis, were incident on the chiral nanowire. Both scattering boundary conditions and perfectly matched layers were used in the outermost domains to prevent backscattered fields. In this way, we are able to calculate scattering (σ_{scat}) and absorption (σ_{abs}) cross-sections associated with the nanowire for incident RCP and LCP light. The extinction cross-section was then calculated as: $\sigma_{\text{ext}} = \sigma_{\text{abs}} + \sigma_{\text{scat}}$. With this information, we calculated the extinction CD signal as: $\text{CD}_{\text{ext}} = \sigma_{\text{ext, LCP}} - \sigma_{\text{ext, RCP}}$.

Author Contributions:

Conceptualization: PS, ES

Project administration: PS, ES

Formal analysis: PS, ES, LKK, CVC

Validation: PS, ES

Funding acquisition: PS, ES

Visualization: PS, ES

Investigation: PS, ES, LKK, CVC

Writing – original draft: PS, ES

Methodology: PS, ES, LKK, CVC

Writing – review & editing: PS, ES, LKK, CVC

Acknowledgements. This work was supported by the U.S. Department of Energy, Office of Science, Office of Basic Energy Sciences under Grant DE-SC0023437. Simulations were supported by the Department of the Navy, Office of Naval Research under ONR award number N00014-20-1-2305. The authors would like to acknowledge C. Argyropoulos for helpful discussions and U. Kilic for technical assistance.

Conflicts of Interests. There are no conflicts of interest to declare.

References

1. L. A. Warning, A. R. Miandashti, L. A. McCarthy, Q. Zhang, C. F. Landes and S. Link, *ACS Nano*, 2021, **15**, 15538-15566.
2. M. Hentschel, M. Schäferling, X. Duan, H. Giessen and N. Liu, *Science Advances*, 2017, **3**, e1602735.
3. F. J. Rodríguez-Fortuño, G. Marino, P. Ginzburg, D. O'Connor, A. Martínez, G. A. Wurtz and A. V. Zayats, *Science*, 2013, **340**, 328-330.
4. H. J. Kimble, *Nature*, 2008, **453**, 1023-1030.
5. P. Lodahl, S. Mahmoodian, S. Stobbe, A. Rauschenbeutel, P. Schneeweiss, J. Volz, H. Pichler and P. Zoller, *Nature*, 2017, **541**, 473-480.
6. H. Pichler, S. Choi, P. Zoller and M. D. Lukin, *Proceedings of the National Academy of Sciences*, 2017, **114**, 11362-11367.
7. H. Coles and S. Morris, *Nature Photonics*, 2010, **4**, 676-685.
8. W. Li, Z. J. Coppens, L. V. Besteiro, W. Wang, A. O. Govorov and J. Valentine, *Nature Communications*, 2015, **6**, 8379.
9. A. Y. Zhu, W. T. Chen, A. Zaidi, Y.-W. Huang, M. Khorasaninejad, V. Sanjeev, C.-W. Qiu and F. Capasso, *Light: Science & Applications*, 2018, **7**, 17158-17158.
10. R. J. Coles, D. M. Price, J. E. Dixon, B. Royall, E. Clarke, P. Kok, M. S. Skolnick, A. M. Fox and M. N. Makhonin, *Nature Communications*, 2016, **7**, 11183.
11. A. S. Baimuratov, I. D. Rukhlenko, Y. K. Gun'ko, A. V. Baranov and A. V. Fedorov, *Nano Letters*, 2015, **15**, 1710-1715.
12. A. S. Baimuratov, I. D. Rukhlenko, R. E. Noskov, P. Ginzburg, Y. K. Gun'ko, A. V. Baranov and A. V. Fedorov, *Scientific Reports*, 2015, **5**, 14712.
13. J. D. Eshelby, *Journal of Applied Physics*, 1953, **24**, 176-179.
14. P. Sutter, S. Wimer and E. Sutter, *Nature*, 2019, **570**, 354-357.
15. P. Sutter, J.-C. Idrobo and E. Sutter, *Advanced Functional Materials*, 2021, **31**, 2006412.
16. Z. Wu, Y. Liu, E. H. Hill and Y. Zheng, *Nanoscale*, 2018, **10**, 18096-18112.
17. C.-J. Kim, A. Sánchez-Castillo, Z. Ziegler, Y. Ogawa, C. Noguez and J. Park, *Nature Nanotechnology*, 2016, **11**, 520-524.
18. L. Hu, H. Huang, Z. Wang, W. Jiang, X. Ni, Y. Zhou, V. Zielasek, M. G. Lagally, B. Huang and F. Liu, *Physical Review Letters*, 2018, **121**, 066401.

19. S. Rex and R. Willa, *New Journal of Physics*, 2022, **24**, 053057.
20. M. N. Chernodub and M. A. Zubkov, *Physical Review B*, 2017, **95**, 115410.
21. H. Sumiyoshi and S. Fujimoto, *Physical Review Letters*, 2016, **116**, 166601.
22. Y. Ran, Y. Zhang and A. Vishwanath, *Nature Physics*, 2009, **5**, 298-303.
23. M. Li, Y. Tsurimaki, Q. Meng, N. Andrejevic, Y. Zhu, G. D. Mahan and G. Chen, *New Journal of Physics*, 2018, **20**, 023010.
24. M. Li, *Journal of Physics: Condensed Matter*, 2019, **31**, 083001.
25. C.-L. Fu and M. Li, *Journal of Physics: Condensed Matter*, 2017, **29**, 325702.
26. S. Hu, H. Zhang, S. Xiong, H. Zhang, H. Wang, Y. Chen, S. Volz and Y. Ni, *Physical Review B*, 2019, **100**, 075432.
27. N. Y. Fogel, A. S. Pokhila, Y. V. Bomze, A. Y. Sipatov, A. I. Fedorenko and R. I. Shekhter, *Physical Review Letters*, 2001, **86**, 512-515.
28. R. S. Wagner and W. C. Ellis, *Applied Physics Letters*, 1964, **4**, 89-90.
29. F. C. Frank, *Discussions of the Faraday Society*, 1949, **5**, 48-54.
30. S. Amelinckx, *Nature*, 1951, **167**, 939-940.
31. A. R. Verma, *Philosophical Magazine*, 1951, **42**, 1005-1013.
32. M. J. Bierman, Y. K. A. Lau, A. V. Kvit, A. L. Schmitt and S. Jin, *Science*, 2008, **320**, 1060-1063.
33. E. I. Solomon and A. B. P. Lever, *Inorganic Electronic Structure and Spectroscopy: Methodology*, Wiley, 2006.
34. N. Berova, K. Nakanishi and R. W. Woody, *Circular dichroism: principles and applications*, John Wiley & Sons, 2000.
35. A. S. Baimuratov, T. P. Pereziabova, W. Zhu, M. Y. Leonov, A. V. Baranov, A. V. Fedorov and I. D. Rukhlenko, *Nano Letters*, 2017, **17**, 5514-5520.
36. E. Sutter and P. Sutter, *Small*, 2021, **17**, 2104784.
37. J. W. Strutt and Baron Rayleigh, *The Theory of Sound*, Macmillan, London, 1878.
38. K. J. Vahala, *Nature*, 2003, **424**, 839-846.
39. K. Kim, S. Yoon, M. Seo, S. Lee, H. Cho, M. Meyyappan and C.-K. Baek, *Nature Electronics*, 2019, **2**, 572-579.
40. T. Nobis, E. M. Kaidashev, A. Rahm, M. Lorenz and M. Grundmann, *Physical Review Letters*, 2004, **93**, 103903.
41. C. Tessarek, C. Dieker, E. Spiecker and S. Christiansen, *Japanese Journal of Applied Physics*, 2013, **52**, 08JE09.
42. J. D. Wiley, A. Breitschwerdt and E. Schonherr, *Solid State Commun*, 1975, **17**, 355-359.
43. D. D. Perovic, C. J. Rossouw and A. Howie, *Ultramicroscopy*, 1993, **52**, 353-359.
44. P. Sutter, L. K. Khorashad, C. Argyropoulos and E. Sutter, *Advanced Materials*, 2021, **33**, 2006649.
45. S. G. Telfer, T. M. McLean and M. R. Waterland, *Dalton Transactions*, 2011, **40**, 3097-3108.
46. S. L. McCall, A. F. J. Levi, R. E. Slusher, S. J. Pearton and R. A. Logan, *Applied Physics Letters*, 1992, **60**, 289-291.
47. A. C. Tamboli, E. D. Haberer, R. Sharma, K. H. Lee, S. Nakamura and E. L. Hu, *Nature Photonics*, 2007, **1**, 61-64.
48. T. Nobis and M. Grundmann, *Physical Review A*, 2005, **72**, 063806.
49. K. P. McKenna, *Journal of the American Chemical Society*, 2013, **135**, 18859-18865.
50. H.-M. Benia, P. Myrach, A. Gonchar, T. Risse, N. Nilius and H.-J. Freund, *Physical Review B*, 2010, **81**, 241415.
51. M. Li, W. Cui, M. S. Dresselhaus and G. Chen, *New Journal of Physics*, 2017, **19**, 013033.
52. Y. Kim, S.-Y. Lee, J.-W. Ryu, I. Kim, J.-H. Han, H.-S. Tae, M. Choi and B. Min, *Nature Photonics*, 2016, **10**, 647-652.
53. W. Ma, L. Xu, A. F. de Moura, X. Wu, H. Kuang, C. Xu and N. A. Kotov, *Chemical Reviews*, 2017, **117**, 8041-8093.
54. A. Polman, M. Kociak and F. J. García de Abajo, *Nature Materials*, 2019, **18**, 1158-1171.

55. K. C. Mills, *Thermodynamic Data for Inorganic Sulphides, Selenides and Tellurides*, Butterworths, London, 1974.
56. J. D. Wiley, W. J. Buckel, W. Braun, G. W. Fehrenbach, F. J. Himpsel and E. E. Koch, *Physical Review B*, 1976, **14**, 697-701.